Heliyon 10 (2024) e24547

Contents lists available at ScienceDirect

Heliyon

journal homepage: www.cell.com/heliyon

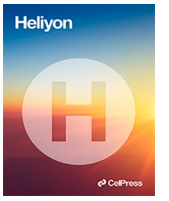

Research article

Improved detection of aortic dissection in non-contrast-enhanced chest CT using an attention-based deep learning model

Fenglei Dong [a], Jiao Song [a], Bo Chen [a], Xiaoxiao Xie [a], Jianmin Cheng [a], Jiawen Song [a], Qun Huang [b,*]

[a] *Department of Radiology, The Second Affiliated Hospital and Yuying Children's Hospital of Wenzhou Medical University, 1111 east section of Wenzhou avenue, Longwan District, Wenzhou, China*
[b] *Department of Radiology, The First Affiliated Hospital of Wenzhou Medical University, No. 1 Fanhai West Road, Ouhai District, Wenzhou, China*

ARTICLE INFO

Keywords:
Aortic dissection
Deep learning
Attention mechanism
Non-contrast-enhanced chest CT

ABSTRACT

Rationale and objectives: This study investigated the effects of implementing an attention-based deep learning model for the detection of aortic dissection (AD) using non-contrast-enhanced chest computed tomography (CT).

Materials and methods: We analysed the records of 1300 patients who underwent contrast-enhanced chest CT at 2 medical centres between January 2015 and February 2023. We considered an internal cohort of 200 patients with AD and 200 patients without AD and an external test cohort of 40 patients with AD and 40 patients without AD. The internal cohort was divided into training and test sets, and a deep learning model was trained using 9600 CT images. A convolutional block attention module (CBAM) and a traditional deep learning architecture (namely, You Only Look Once version 5 [YOLOv5]) were combined into an attention-based model (i.e., YOLOv5-CBAM). Its performance was measured against the unmodified YOLOv5 model, and the accuracy, sensitivity, and specificity of the algorithm were evaluated by two independent radiologists.

Results: The CBAM-based model outperformed the traditional deep learning model. In the external testing set, YOLOv5-CBAM achieved an area under the curve (AUC) of 0.938, accuracy of 91.5 %, sensitivity of 90.0 %, and specificity of 92.9 %, whereas the unmodified model achieved an AUC of 0.844, accuracy of 83.6 %, sensitivity of 71.2 %, and specificity of 96.0 %. The sensitivity results of the unmodified algorithms were not significantly different from those of the radiologists; however, the proposed YOLOv5-CBAM algorithm outperformed the unmodified algorithms in terms of detection.

Conclusions: Incorporating the CBAM attention mechanism into a deep learning model can significantly improve AD detection in non-contrast-enhanced chest CT. This approach may aid radiologists in the timely and accurate diagnosis of AD, which is important for improving patient outcomes.

* Corresponding author.
E-mail addresses: nt39015251@sina.com (F. Dong), 791632195@qq.com (J. Song), xncyxchenb@163.com (B. Chen), 27672877@qq.com (X. Xie), chengjm@wzhealth.com (J. Cheng), 2290338196@qq.com (J. Song), dr_wongq@wzhospital.cn (Q. Huang).

https://doi.org/10.1016/j.heliyon.2024.e24547
Received 17 June 2023; Received in revised form 22 December 2023; Accepted 10 January 2024
Available online 17 January 2024

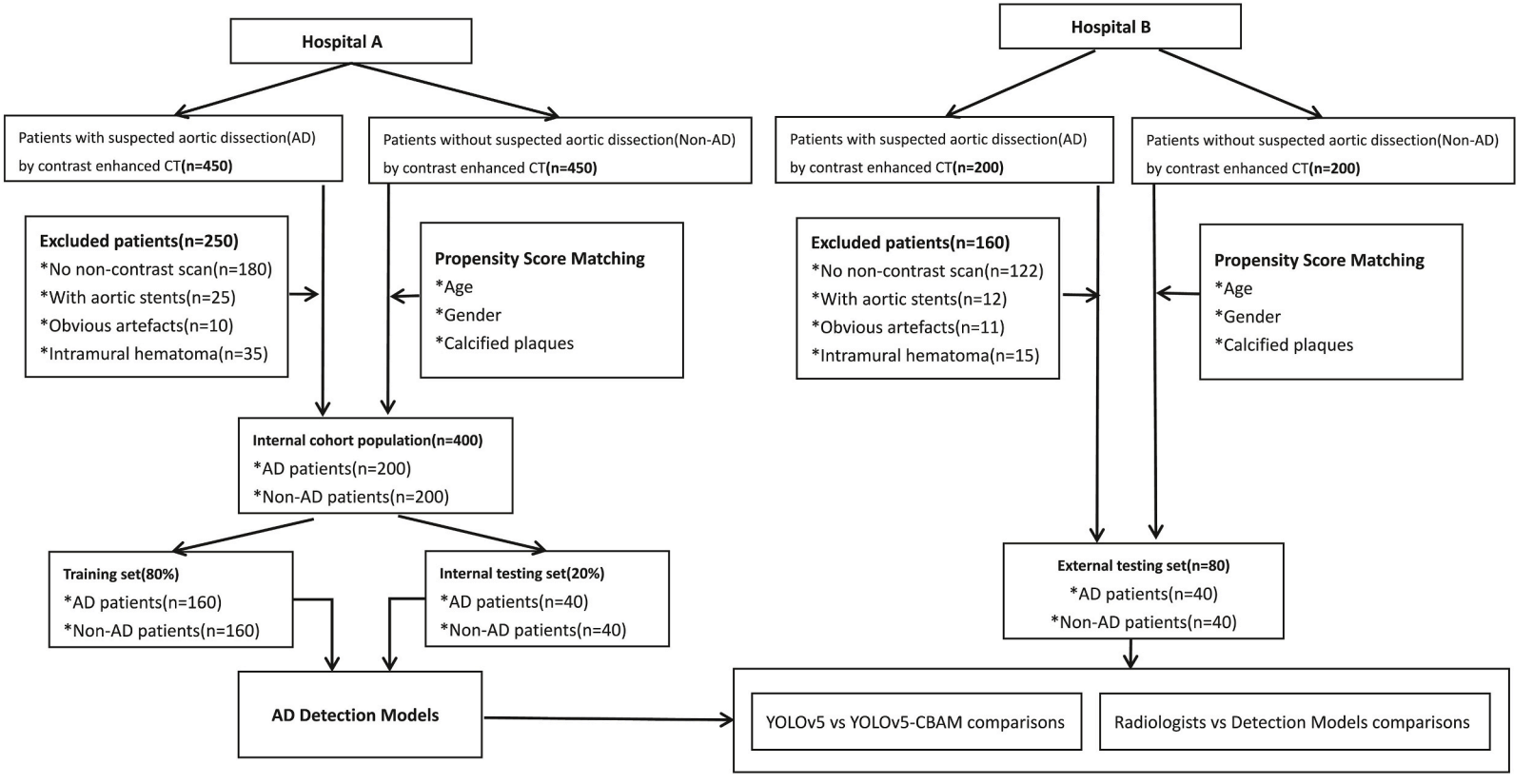

Fig. 1. Flowchart illustrates the study design.

1. Introduction

Aortic dissection (AD) is a fatal medical emergency and occurs when a tear forms in the inner layer of the aortic wall, which causes blood to flow into a false lumen within the aortic wall [1]. The true incidence of AD is difficult to determine owing to its sudden onset and high mortality rate, but it is estimated to occur in approximately 2.6–3.5 individuals per 100,000 individuals annually, with men being more commonly affected than women [2]. The cause of AD is unknown; however, it may be associated with factors such as hypertension, history of aortic or aortic valve disease, family history of aortic disease, history of heart surgery, and smoking. The symptoms of AD include intense pain in the chest, back, and abdomen accompanied by shortness of breath, sweating, and fainting [3, 4].

The accurate and rapid diagnosis of AD depends heavily on imaging techniques, including magnetic resonance imaging (MRI), computed tomography angiography (CTA), and echocardiography [5]. Echocardiography is quick and convenient; however, its accuracy may be limited by factors such as narrow intercostal spaces, obesity, emphysema, and operator skill and experience. MRI is also a major technique for diagnosing AD because of its high sensitivity and specificity. However, the lengthy scan time and unfavourable logistics make it unsuitable for emergency AD examinations [6]. CTA is the preferred method owing to its high scanning speed, accessibility, and diagnostic accuracy. However, one disadvantage of CTA is that the contrast agent may be nephrotoxic, thus making it unsuitable for patients with impaired renal function or allergies to contrast agents [7].

Non-contrast-enhanced computed tomography (CT) scans may reveal features such as aortic wall thickening, displaced calcified intimal flaps, and dilated aortic segments and may suggest AD in certain cases [8]. However, the accurate diagnosis of AD using non-contrast-enhanced CT scans remains challenging owing to the potential subtlety and lack of specificity of imaging findings. Deep learning algorithms can learn from subtle differences in image features that may not be apparent to human observers. In the field of medical imaging, deep learning algorithms are being used to support the interpretation and analysis of various types of medical images, such as MRI, CT, and X-ray images [9–12]. Recently, several studies have explored the potential of deep learning algorithms, particularly convolutional neural networks (CNNs), for the automatic detection and classification of AD in non-contrast-enhanced CT images, and the results have been encouraging in terms of both accuracy and efficiency [13–15]. Despite these achievements, previous CNN-based studies on AD detection in chest CT images have limited diagnostic efficiency owing to network insensitivity to small objects, including the aortic region, which constitutes only a small portion of axial chest CT images. To improve diagnostic accuracy and efficiency, there is a need for deep learning techniques that can achieve accurate small-object detection. An attention mechanism can be added to a CNN architecture to enhance important features in an image while suppressing irrelevant features; this approach can result in enhanced accuracy in various computer vision tasks such as object detection, image categorisation, and semantic region identification in images [16–22].

This study is the first to investigate whether the implementation of an attention-based deep learning model can enhance the detection performance of AD in non-contrast-enhanced chest CT images.

2. Materials and methods

The institutional ethics committees of the two hospitals reviewed and approved this study. Owing to the retrospective nature of the study, the requirement for written informed consent was waived.

2.1. Patient population

We conducted a retrospective analysis of 1300 patients who underwent contrast-enhanced chest CT at 2 medical centres between January 2015 and February 2023. In particular, 900 and 400 patients were from hospitals A and B, respectively. The inclusion criteria

Table 1
Patient demographics.

Characteristic	Training set			Internal testing set			External testing set		
	AD	Non-AD	p value	AD	Non-AD	p value	AD	Non-AD	p value
Number of patients	160	160		40	40		40	40	
Stanford type									
A	60			15			15		
B	100			25			25		
Age (mean ± SD)	53.90 ± 13.98	55.61 ± 12.16	0.452	57.85 ± 14.77	58.91 ± 15.11	0.655	52.82 ± 15.63	50.82 ± 14.23	0.562
Gender									
Male	137	141	0.508	30	32	0.592	35	33	0.531
Female	23	19		10	8		5	7	
Number of calcified plaque slices									
<5	125	118	0.360	33	30	0.412	34	35	0.745
≥5	35	42		7	10		6	5	

The p-values were calculated by the Mann-Whitney *U* test or the Pearson's chi-squared test when appropriate.
AD : Aortic Dissection.

were as follows: (a) patients who were diagnosed with AD based on contrast-enhanced CT, (b) patients who underwent non-contrast-enhanced CT scans and contrast-enhanced chest CT on the same day, and (c) patients who did not have aortic stents. Patients with obvious CT image artefacts and those diagnosed with aortic intramural haematoma were excluded from the study. Ultimately, we selected 240 patients with AD and matched them to 240 patients without AD, as confirmed by contrast-enhanced CT, on the basis of age, sex, and calcified plaques in the aortic wall. Among the 400 patients from hospital A, 75 had Stanford type-A AD, 125 had Stanford type-B AD, and 200 had no AD. The patients were randomly divided into a training set (60 Stanford type-A patients, 100 Stanford type-B patients, and 160 non-AD patients [320/400, 80 %]) and an internal testing set (15 Stanford type-A patients, 25 Stanford type-B patients, and 40 non-AD patients [80/400, 20 %]). In addition, 80 patients were selected from hospital B for the external testing set (15 Stanford type-A patients, 25 Stanford type-B patients, and 40 non-AD patients). Fig. 1 shows a flowchart of the process adopted in this study. Table 1 shows a summary of the demographic characteristics of the patients.

2.2. Data collection

Datasets were collected from the electronic medical records of our hospital. The training and internal testing sets comprised images acquired from two different multi-row CT scanners (A and B), whereas images in the external testing set were obtained from three different multi-row CT scanners (C, D, and E). The scanning parameters were as follows: matrix size, 512 × 512; slice thickness, 5 mm; tube voltage, 100–120 kV; and automatically modulated tube current. The CT images were stored in DICOM format and were anonymised prior to inclusion in the study. Non-contrast-enhanced CT images that included both positive and negative cases of AD were examined by two senior radiologists, who independently confirmed the diagnosis of AD. We converted the transverse thoracic CT images of each patient with a window width of 350 Hounsfield units (HU) and a window level of 35 HU into JPEG format. Each image slice was then annotated with bounding boxes around the area of the aorta and labelled with 'AD' or 'non-AD' according to the corresponding contrast-enhanced CT slice. In cases of disagreement, a third senior radiologist was consulted to achieve consensus.

3. Deep learning model

3.1. You Only Look Once version 5 (YOLOv5) algorithm

YOLOv5 is a cutting-edge object detection algorithm that uses deep CNNs for the real-time detection of objects in images and videos. The architecture of YOLOv5 is based on a feature extraction backbone, followed by detection layers that predict the bounding boxes and class probabilities for each detected object (Fig. 2a). The CSPDarknet backbone consists of multiple convolutional layers, including combinations of convolutional and pooling layers. This backbone is used to extract features from the input images, and these

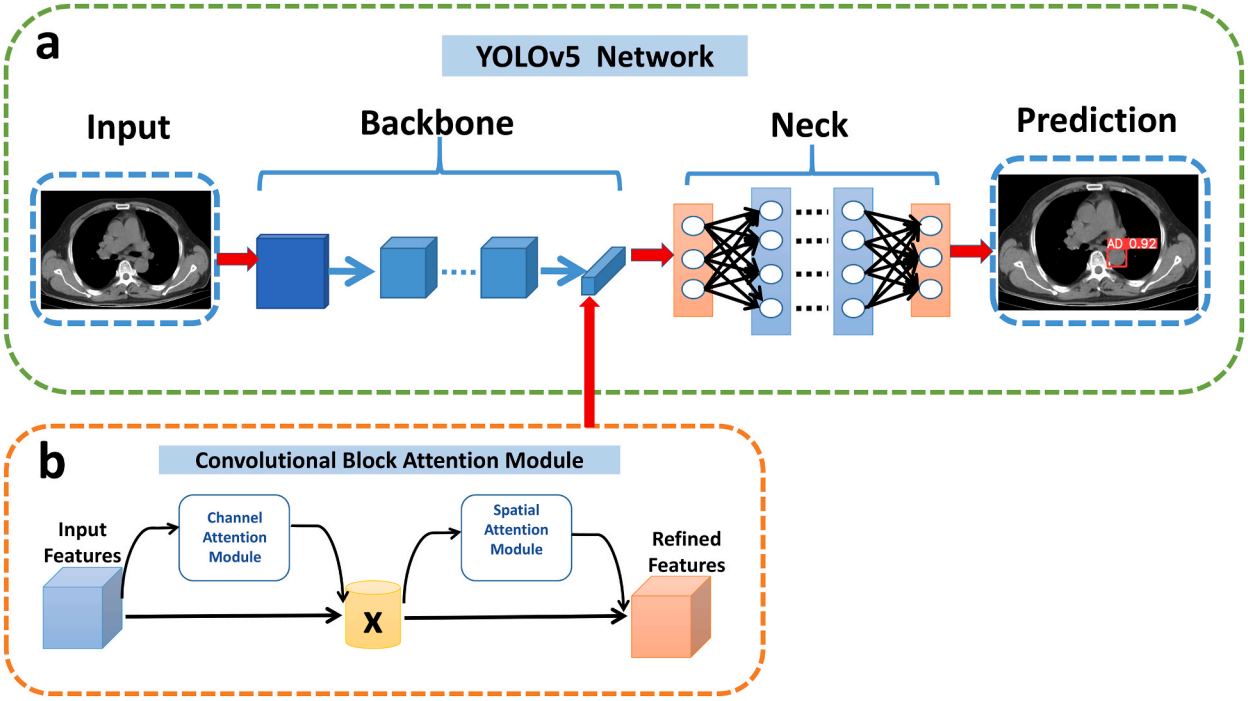

Fig. 2. Outline of deep learning modelling for the prediction of aortic dissection based on non-contrast-enhanced chest CT. (a) An overview of the architecture and detection process of the You Only Look Once version 5 (YOLOv5) model. (b) A convolutional block attention module (CBAM) was added to the backbone of the YOLOv5 model to create a new model (i.e., YOLOv5-CBAM).

features are then used to predict the bounding boxes and class probabilities of each detected object. The detection layers consist of multiple convolutional layers that perform object detection and classification. In this study, the YOLOv5 algorithm was trained using a transfer learning strategy on a large collection of chest CT images. The algorithm was coded using the PyTorch deep learning framework and Python programming language. The hyperparameters of the algorithm were optimised using the Adam optimisation algorithm with a learning rate of 0.001 and batch size of 32. The optimal weight parameters were obtained after 300 training rounds. These parameters were loaded into YOLOV5 to evaluate dataset B.

3.2. Convolutional block attention module (CBAM)

A CBAM was added to the CSPDarknet backbone of the YOLOv5 algorithm to improve detection efficiency (Fig. 2b). CBAM is a type of attention mechanism that enhances important features in an image while suppressing irrelevant features. It incorporates two attention modules for channel and spatial attention. In AD detection, the channel attention module focuses on channels linked to the AD, whereas the spatial attention module reduces the importance of non-aortic regions, which comprise a significant portion of axial chest CT images.

3.3. Gradient-weighted class activation mapping (Grad-CAM)

Grad-CAM is a deep learning technique used for visualising the importance of different areas of an input image for a particular output class [23]. It computes a score gradient for a particular class in relation to the feature maps of the final convolutional layer. The resulting gradient map is then used to produce weighted sum-of-feature maps, which are subsequently processed using an activation function to obtain a final heat map that will be overlaid on an input image. The colour intensity in each region of the heat map indicates the level of importance of that region for classification. A higher colour intensity corresponds to the higher importance of the region for classification.

4. Experiments

To establish the efficacy of our model, we conducted two distinct experiments for comparison. In the first experiment, we used an unmodified YOLOv5 algorithm. In the second experiment, we used the YOLOv5-CBAM model, in which the CBAM was integrated into the YOLOv5 algorithm. Both models were trained and validated internally on dataset A and externally on dataset B. The algorithms processed the input images and subsequently produced the bounding boxes and confidence scores for each detected object. The confidence score represents the probability that a detected object represents an AD. A higher confidence score indicates that the model is more confident that an object represents AD. For each detected object, we compared the confidence score to the ground-truth label (‘AD’ or ‘non-AD’) to determine if it was a true positive, false positive, true negative, or false negative. The confidence threshold used to determine whether an object was considered to represent AD varied, and the true-positive rate (TPR) and false-positive rate (FPR) were computed for each threshold. Receiver operating characteristic curves were obtained by plotting the TPR against the FPR at varying thresholds.

4.1. Radiologist performance

Two radiologists specialising in cardiovascular imaging with 8 and 10 years of experience, respectively, compared the algorithms by using their diagnostic abilities. We utilised transverse non-contrast-enhanced chest CT images in DICOM format, which were randomised and anonymised with an adjustable window level of 30 HU and a width of 400 HU. Both internal and external testing sets were used. The radiologists independently reviewed each image and provided a diagnosis of ‘AD’ or ‘non-AD’. A third radiologist compared these diagnoses to the ground-truth labels of ‘AD’ or ‘non-AD’ to determine whether they were true positives, false positives, true negatives, or false negatives.

4.2. Statistical analysis

Statistical analyses were conducted using Python and R programming languages (version 4.1.3, https://www.r-project.org/). To examine the differences in demographic characteristics and CT findings between patients, we conducted independent t-tests or Mann–Whitney U-tests for continuous variables and Fisher’s exact tests or chi-square tests for categorical variables.

To determine whether the performance of the two algorithms was superior to the average performance of the radiologists, we used Pearson’s chi-square test to compare the accuracy, sensitivity, and specificity of the classification models. We also employed Fleiss’s kappa coefficient to evaluate the inter-rater agreement between the two radiologists.

To assess the detection performance of the two algorithms, we calculated the area under the curve (AUC), sensitivity, specificity, and accuracy and compared the two AUC values by using the DeLong method. A threshold of 0.05 was considered statistically significant.

5. Results

We trained two deep learning models, namely, YOLOv5 and YOLOv5-CBAM, to detect AD in non-contrast-enhanced chest CT scans.

The models were trained using averages of 9600, 2400, and 2500 images (11,100, 3280, and 3226 regions of interest) for training, internal testing, and external testing, respectively. The processing times for the internal and external testing were 67 and 70 s (0.028 s/slice), respectively.

Table 2 presents the experimental results. In the internal testing set, there was no statistically significant difference in the AUC values between YOLOv5 and YOLOv5-CBAM for detecting Stanford type-A or type-B AD (**Table 2**). In the external testing set, YOLOv5-CBAM outperformed YOLOv5 in detecting type-A AD with a detection threshold of 0.03, as evidenced by its higher AUC (0.905 versus 0.828) and sensitivity (0.842 versus 0.681); however, there was a slight reduction in its specificity from 0.965 to 0.932. Similarly, YOLOv5-CBAM exhibited superior performance in detecting type-B AD with a higher AUC (0.964 versus 0.857) and sensitivity (0.946 versus 0.737); however, its specificity decreased slightly from 0.957 to 0.927. Furthermore, when detecting both type-A and type-B ADs, YOLOv5-CBAM exhibited improved performance compared with YOLOv5, with an increased AUC of 0.938 and sensitivity of 0.900. By contrast, YOLOv5 achieved lower values of 0.844 and 0.712 for these parameters. However, the specificity of YOLOv5-CBAM (0.929) was slightly lower than that of YOLOv5 (0.960) (Table 2, Figs. 3 and 4).

On the internal and external testing sets, Fleiss's kappa coefficients between the two radiologists were 0.85 and 0.78, respectively, which suggested a high level of agreement. In the internal testing set, both the YOLOv5 and YOLOv5-CBAM algorithms exhibited significant differences in accuracy, sensitivity, and specificity compared with the two radiologists. However, in the external testing set, the YOLOv5 algorithm exhibited no statistically significant differences in sensitivity when compared with the evaluations of the two radiologists, whereas the YOLOv5-CBAM algorithm outperformed the radiologists in terms of detection performance (Table 2, Figs. 3 and 4).

Fig. 5 shows representative examples of lesion detection by the YOLOv5 and YOLOv5-CBAM models.

6. Discussion

We developed and validated a deep learning algorithm that utilises an attention mechanism for the automatic detection of thoracic AD in non-contrast-enhanced CT images. In detecting both type-A and type-B ADs on the external testing set, the developed model outperformed two experienced radiologists with an AUC of 0.938, accuracy of 0.915, sensitivity of 0.900, and specificity of 0.929.

Table 2
Diagnostic ability of the deep learning models and radiologists for the internal and external testing set.

	AUC	95%CI	Accuracy (%)	Sensitivity (%)	Specificity (%)
Internal testing set					
Stanford type A					
YOLOv5	0.974	0.964–0.984	97.1	96.6	97.7
YOLOv5-CBAM	0.984	0.977–0.991	97.1	97.1	97.2
Radiologist 1			76.5$^{\#\$}$	66.5$^{\#\$}$	86.5$^{\#\$}$
Radiologist 2			80.9$^{\#\$}$	73.3$^{\#\$}$	88.5$^{\#\$}$
Stanford type B					
YOLOv5	0.976	0.967–0.986	97.7	97.2	98.1
YOLOv5-CBAM	0.990	0.985–0.995	98.5	98.1	98.8
Radiologist 1			79.4$^{\#\$}$	73.1$^{\#\$}$	85.8$^{\#\$}$
Radiologist 2			82.4$^{\#\$}$	75.6$^{\#\$}$	89.2$^{\#\$}$
Type A + B					
YOLOv5	0.975	0.968–0.987	97.4	96.9	97.9
YOLOv5-CBAM	0.987	0.983–0.992	97.9	97.8	98.1
Radiologist 1			78.1$^{\#\$}$	70.1$^{\#\$}$	86.2$^{\#\$}$
Radiologist 2			81.7$^{\#\$}$	74.6$^{\#\$}$	88.9$^{\#\$}$
External testing set					
Stanford type A					
YOLOv5	0.828	0.806–0.851	82.3	68.1	96.5
YOLOv5-CBAM	0.905*	0.888–0.922	88.7	84.2	93.2
Radiologist 1			77.5$^{\$}$	67.5$^{\$}$	87.5$^{\#\$}$
Radiologist 2			80.2$^{\$}$	71.2$^{\$}$	89.3$^{\#\$}$
Stanford type B					
YOLOv5	0.857	0.838–0.875	84.7	73.7	95.7
YOLOv5-CBAM	0.964*	0.955–0.974	93.6	94.6	92.7
Radiologist 1			78.4$^{\$}$	71.5$^{\$}$	85.3$^{\#\$}$
Radiologist 2			80.9$^{\$}$	73.2$^{\$}$	88.7$^{\#\$}$
Type A + B					
YOLOv5	0.844	0.830–0.858	83.6	71.2	96.0
YOLOv5-CBAM	0.938*	0.928–0.947	91.5	90.0	92.9
Radiologist 1			78.0$^{\$}$	69.7$^{\$}$	86.2$^{\#\$}$
Radiologist 2			80.6$^{\$}$	72.3$^{\$}$	89.0$^{\#\$}$

*$p < 0.05$, comparison between the YOLOv5 and YOLOv5-CBAM by the DeLong test.
$^{\#}p < 0.05$, comparison between the YOLOv5 and each radiologist by the Pearson's chi-squared test.
$^{\$}p < 0.05$, comparison between the YOLOv5-CBAM and each radiologist by the Pearson's chi-squared test.

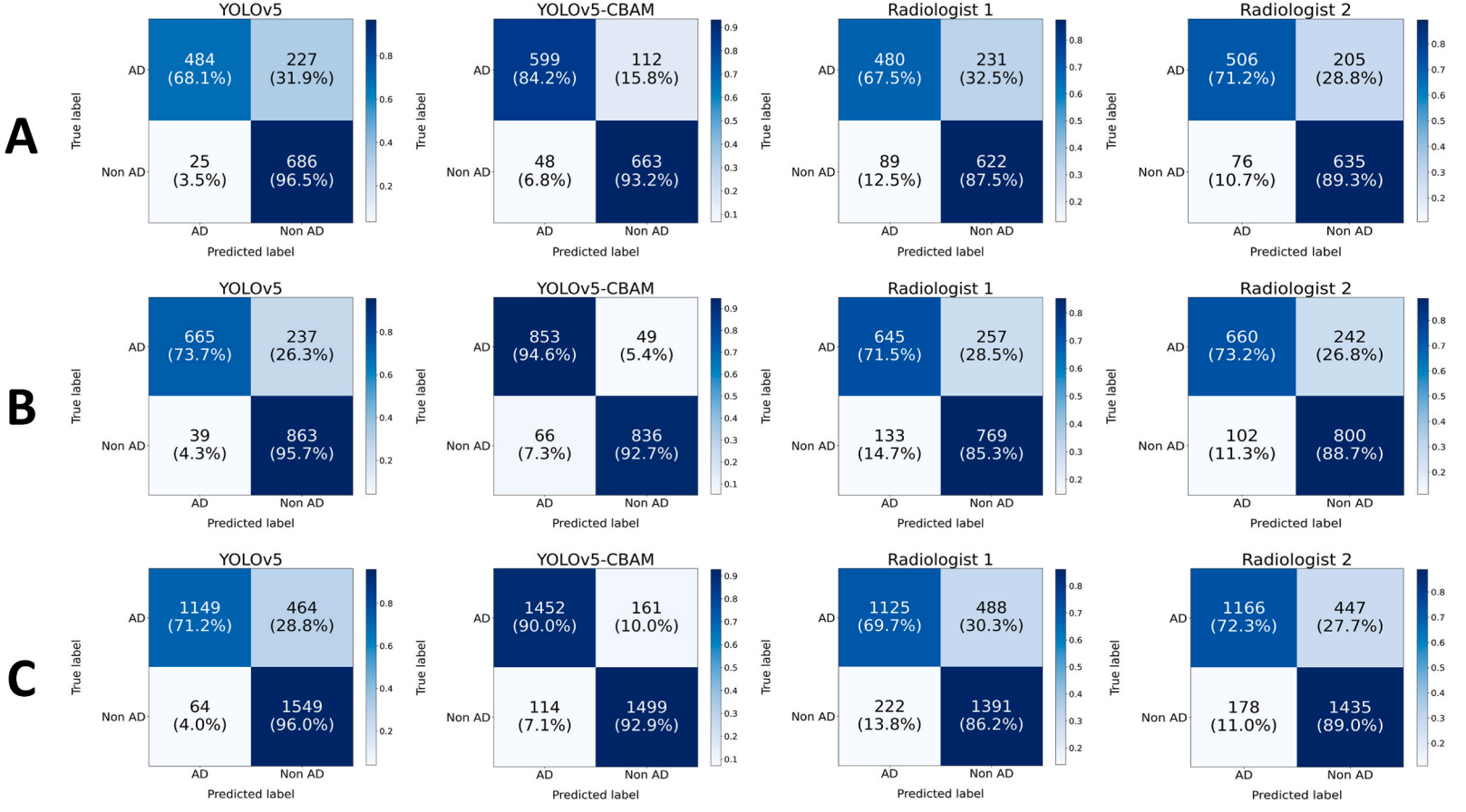

Fig. 3. Confusion matrices comparing the diagnostic performance of deep learning models and radiologists in the external testing set for Stanford type A (A), Stanford type B (B), and both types combined (C). The confusion matrices show the numbers of true positive (TP), false positive (FP), false negative (FN), and true negative (TN) cases for each group, thus allowing for the evaluation of the performance of the models and radiologists in the identification of the different types of cases.

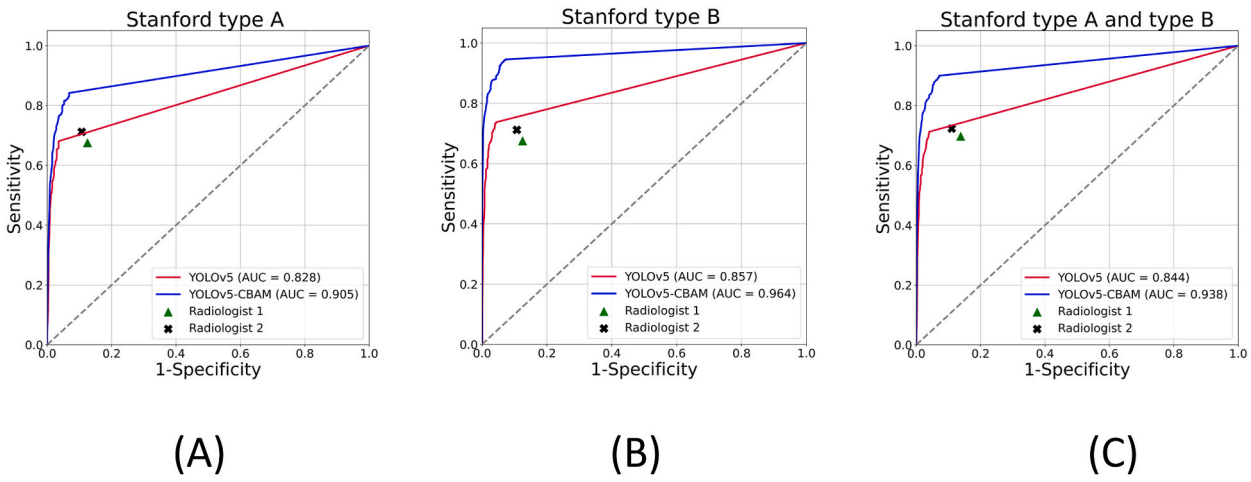

Fig. 4. Receiver operating characteristic curves comparing the diagnostic performance of deep learning models and radiologists in the external testing set for Stanford type A (A), Stanford type B (B), and both types combined (C).

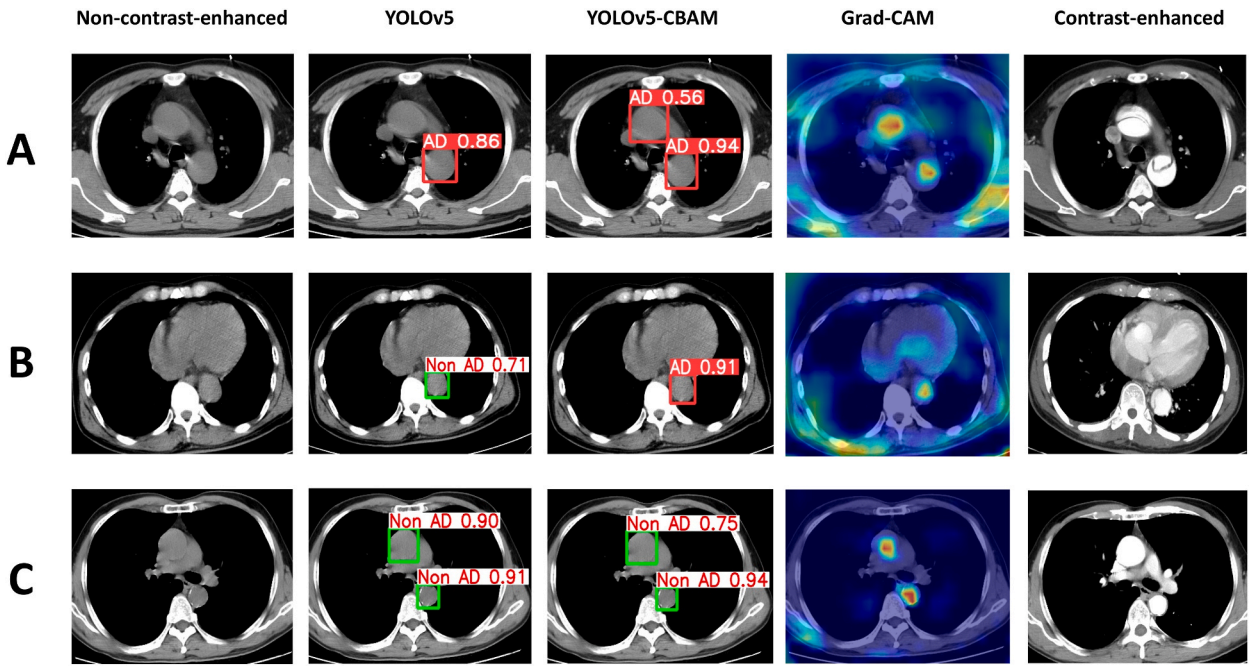

Fig. 5. Representative examples of lesion detection by the You Only Look Once version 5 (YOLOv5) model and combined YOLOv5 and convolutional block attention module (YOLOv5-CBAM) model. (A) YOLOv5-CBAM successfully detected Stanford type A aortic dissection in a 50-year-old man, whereas YOLOv5 failed to detect the lesion of the ascending aorta. (B) YOLOv5-CBAM successfully detected Stanford type B aortic dissection in a 56-year-old man, whereas the YOLOv5 misdiagnosed the lesion as non-aortic dissection. (C) Both the YOLOv5-CBAM and YOLOv5 models correctly identified the aortic dissection of a 58-year-old man as negative.

These results indicate that the YOLOv5-CBAM model is robust and highly accurate in detecting AD and can be implemented as a useful tool in clinical practice.

Several studies have explored the potential of deep learning algorithms for the automatic detection and classification of AD in non-contrast-enhanced CT images. Hata et al. [13] utilised a deep learning model based on the Xception architecture to detect AD in non-contrast-enhanced CT scans. Their approach yielded promising outcomes that are comparable to the diagnostic performance of radiologists. Although this model classified the entire image slices, it did not focus on the aortic area. This could lead to an increased likelihood of false positives if the input images do not feature the aorta or if other lesions are present in the input images, such as pneumonia or pleural effusion. To overcome this problem, Hata et al. [13] designed an additional algorithm to detect the aorta, thus resulting in a more complex workflow. Yi et al. [14] proposed a novel approach for predicting AD by combining a Gaussian/naïve

Bayes–based deep learning scoring function with morphological features. Although effective, this method requires multiple time-consuming training steps and does not provide detection results for every CT image slice. By contrast, the proposed algorithm requires only a single training step. This architecture can simultaneously locate and identify lesions by leveraging the context of input images. Additionally, the detection results were visualised by displaying coloured bounding boxes in the original images with associated confidence values.

Although there were no significant differences in the AUC values between YOLOv5 and YOLOv5-CBAM on the internal testing set, YOLOv5 exhibited a noticeable decrease in detection performance on the external testing set compared with YOLOv5-CBAM, which only experienced a slight decrease. These differences can be attributed to variations in the data distribution and imaging characteristics between the two sets. The internal cohort comprised cases from two machines, whereas the external cohort included cases from three machines. Variations in scanner type, imaging protocol, and image quality may have contributed to the observed performance differences. Moreover, deep learning models often risk overfitting owing to an extensive parameter count, thus resulting in good performance on internal testing sets but poor performance on external testing sets. However, the YOLOv5-CBAM model effectively improves its ability to generalise external data by enhancing important image features and suppressing irrelevant features. This improved focus leads to increased sensitivity but also introduces a slight decrease in specificity. The model is more sensitive in detecting AD, but the trade-off is a slightly higher likelihood of false positives. We believe that this trade-off is acceptable given the potential clinical benefits of early detection and treatment.

Studies [1,2] have demonstrated that the Stanford classification system is particularly useful for guiding treatment decisions because it facilitates the identification of patients who may benefit from surgical interventions. Given that our model can process each slice of an axial chest CT image, it can detect both Stanford types A and B in non-contrast-enhanced CT scans. Therefore, our model can facilitate early detection and prompt treatment. However, additional contrast-enhanced CT scans may be necessary for a more comprehensive evaluation. When attempting to detect type-A AD, the performance of YOLOv5 is relatively poor, which can be attributed to the presence of calcified plaques on the aortic arch wall and motion artefacts at the aortic root, thus leading to misclassification. In addition, because there are more complex adjacent structures around the ascending aortic root than around the descending aorta, YOLOv5 may fail to identify the structure of the ascending aorta (Fig. 5a). Further investigations are required to understand the underlying reasons for the performance variations of the model between the two types of AD.

This study has several limitations. First, there may have been selection bias because all included patients required both a plain chest CT scan and contrast-enhanced CT within 24 h. Furthermore, many cases of AD were initially diagnosed using CTA, and this diagnosis is not possible when using traditional CT. Second, the sample size was small, and data were only collected from two medical centres; these factors could limit data diversity and affect the generalizability of our algorithm. Therefore, further research with larger multicentre samples is necessary. Third, the CT scans used in this study were obtained from different suppliers and their imaging quality may not have been consistent, which could have affected the detection results. However, this may reflect the reality of clinical settings in which various CT brands are used. Finally, the detection of type-A AD still poses additional challenges because of motion artefacts at the aortic root, significant calcified plaques in the aortic arch, and the anatomical location of the ascending aorta. Further research and development are required to address these issues.

In conclusion, although contrast-enhanced CT is the prevailing diagnostic method for AD, the ability to diagnose AD by using non-contrast-enhanced CT is crucial for patients who are unable to tolerate contrast agents owing to renal toxicity and in clinical scenarios wherein contrast-enhanced CT is not feasible. Our study successfully integrated CBAM into the YOLOv5 algorithm, thus leading to improved detection efficiency for AD in non-contrast-enhanced chest CT images compared to the performance of experienced radiologists. Our approach can effectively identify different types of AD and facilitate the early disease detection and optimisation of clinical decisions.

Ethics statement

Ethics approval was granted by the Ethics Committee in Clinical Research of the First Affiliated Hospital of Wenzhou Medical University, with approval number KY2023-R056.

Funding This study has received funding by Science and Technology Plan Project of Wenzhou, China (No. Y20220442).

Data availability statement

Data associated with the study has not been deposited into a publicly available repository and data will be made available on request.

CRediT authorship contribution statement

Fenglei Dong: Writing – original draft, Software, Project administration, Investigation, Funding acquisition. **Jiao Song:** Project administration, Investigation. **Bo Chen:** Data curation. **Xiaoxiao Xie:** Data curation. **Jianmin Cheng:** Validation, Formal analysis. **Jiawen Song:** Formal analysis. **Qun Huang:** Writing – review & editing, Visualization, Resources, Methodology, Conceptualization.

Declaration of competing interest

The authors declare that they have no known competing financial interests or personal relationships that could have appeared to

influence the work reported in this paper.

References

[1] T. Carrel, et al., Acute aortic dissection, Lancet 401 (10378) (2023) 773–788.
[2] B. Rylski, O. Schilling, M. Czerny, Acute aortic dissection: evidence, uncertainties, and future therapies, Eur. Heart J. 44 (10) (2023) 813–821.
[3] I. Hameed, A.S. Cifu, P. Vallabhajosyula, Management of thoracic aortic dissection, JAMA 329 (9) (2023) 756–757.
[4] E. Bossone, K.A. Eagle, Epidemiology and management of aortic disease: aortic aneurysms and acute aortic syndromes, Nat. Rev. Cardiol. 18 (5) (2021) 331–348.
[5] E. Keller Saadi, Multidetector computed tomography scanning is still the gold standard for diagnosis of acute aortic syndromes, Interact. Cardiovasc. Thorac. Surg. 11 (3) (2010) 359.
[6] T. Shiga, et al., Diagnostic accuracy of transesophageal echocardiography, helical computed tomography, and magnetic resonance imaging for suspected thoracic aortic dissection: systematic review and meta-analysis, Arch. Intern. Med. 166 (13) (2006) 1350–1356.
[7] M.M. Ciccone, et al., Advances in the diagnosis of acute aortic syndromes: role of imaging techniques, Vasc. Med. 21 (3) (2016) 239–250.
[8] M.A. McMahon, C.A. Squirrell, Multidetector CT of aortic dissection: a pictorial review, Radiographics 30 (2) (2010) 445–460.
[9] B.N. Dontchos, et al., External validation of a deep learning model for predicting mammographic breast density in routine clinical practice, Acad. Radiol. 28 (4) (2021) 475–480.
[10] A. Esteva, et al., A guide to deep learning in healthcare, Nat. Med. 25 (1) (2019) 24–29.
[11] T. Ueda, et al., Deep learning reconstruction of diffusion-weighted MRI improves image quality for prostatic imaging, Radiology 303 (2) (2022) 373–381.
[12] P.L. Kuo, Y.J. Wu, F.Z. Wu, Pros and cons of applying deep learning automatic scan-range adjustment to low-dose chest CT in lung cancer screening programs, Acad. Radiol. 29 (10) (2022) 1552–1554.
[13] A. Hata, et al., Deep learning algorithm for detection of aortic dissection on non-contrast-enhanced CT, Eur. Radiol. 31 (2) (2021) 1151–1159.
[14] Y. Yi, et al., Advanced warning of aortic dissection on non-contrast CT: the combination of deep learning and morphological characteristics, Front Cardiovasc Med 8 (2021) 762958.
[15] W.T. Liu, et al., A deep-learning algorithm-enhanced system integrating electrocardiograms and chest X-rays for diagnosing aortic dissection, Can. J. Cardiol. 38 (2) (2022) 160–168.
[16] N. Mao, et al., Attention-based deep learning for breast lesions classification on contrast enhanced spectral mammography: a multicentre study, Br. J. Cancer 128 (5) (2023) 793–804.
[17] A.G.C. Pacheco, R.A. Krohling, An attention-based mechanism to combine images and metadata in deep learning models applied to skin cancer classification, IEEE J Biomed Health Inform 25 (9) (2021) 3554–3563.
[18] Y. Zhang, et al., Brain tumors classification for MR images based on attention guided deep learning model, Annu Int Conf IEEE Eng Med Biol Soc 2021 (2021) 3233–3236.
[19] X. Cao, et al., Swin-transformer-based YOLOv5 for small-object detection in remote sensing images, Sensors 23 (7) (2023).
[20] S. Chen, et al., Automatic detection of stroke lesion from diffusion-weighted imaging via the improved YOLOv5, Comput. Biol. Med. 150 (2022) 106120.
[21] Y. Luo, et al., Intelligent solutions in chest abnormality detection based on YOLOv5 and ResNet 50, J Healthc Eng 2021 (2021) 2267635.
[22] S. Woo, et al., Cbam: convolutional block attention module, in: Proceedings of the European Conference on Computer Vision, ECCV), 2018.
[23] R.R. Selvaraju, et al., Grad-cam: visual explanations from deep networks via gradient-based localization, in: Proceedings of the IEEE International Conference on Computer Vision, 2017.